Electronic Supplementary Material (ESI) for Chemical Communications.

Electronic Supplementary information (EIS) for

Electrochemical performances and reaction kinetics of an longer linear ligand based MOF as a novel anode material for sodium-ion batteries

Yan Zhang,[a] Shihui Yang,[b] Xiaoya Chang,[a] Huinan Guo,[a] Yunwei Li,[a] Mengying Wang,[a] Weiqin Li,[a] Lifang Jiao,[a] and Yijing Wang*[a]

[a] *Key Laboratory of Advanced Energy Materials Chemistry (Ministry of Education), College of Chemistry, Nankai University, Tianjin 300071, P. R. China.*

* *Corresponding author, E-mail: wangyj@nankai.edu.cn.*

[b] *State Key Laboratory of Advanced Power Transmission Technology (Global Energy Interconnection Research Institute Co.,LTD), Changping District, Beijing 102209, P. R. China.*

Experimental section

Synthesis of Co-bpdc MOF

Typically, 0.55 mmol H_2bpdc was deprotonated by sodium hydroxide (1.1 mmol) in 15 mL water. After a solution (30 mL) of $Co(NO_3)\cdot 6H_2O$ (3 mmol) added, white pink precipitate appeared rapidly. The precipitate was centrifuged, washed using N, N-dimethyl formamide (DMF) and water (2 times, respectively) and then dried overnight in vacuum at 80 °C.

Characterization

The obtained samples were characterized by powder X-ray diffractometry (XRD) using a Rigaku MiniFlex II diffractometer equipped with a Cu target at a scan rate of 4° min^{-1}. The Fourier transforming infrared (FT-IR) spectra measurement was conducted on a FTIR-650 (Tianjin Gangdong). The thermo-gravimetric (TG) curve was obtained in air from a thermal analyser (Labsys evo, Setram Instrumentation, France). X-ray photoelectron spectroscopy (XPS) was performed on a PHI5000VersaProbe system (ULVCA-PHI, Japan). Field-emission electron microscopy (FESEM) and Transmission electron microscopy (TEM) images were obtained from a JEOL JSM-7500F and JEM-2100, respectively.

Electrochemical testing

For electrochemical testing, the anode materials were evaluated in 2032-type coin cells using a Na disk as the counter electrode and 1 M $NaClO_4$ in propylene carbonate (PC) with 5% fluoroethylene carbonate (FEC) solution as the electrolyte. The work electrodes were prepared by mixing a composite of active materials (60 wt%), Super P carbon black (30 wt%) and carboxymethyl cellulose (CMC, 10 wt%) and dispersing in de-ionized water to form an homogeneous slurry. Then the slurry was cast onto a copper foil collector and dried overnight in vacuum at 80 °C. The typical loading of active materials was approximately 1.5 mg cm^{-1}. Assembly of the cells was carried out in a dry Ar-filled glove box (oxygen and water concentration less than 0.1 ppm, Mikrouna). Galvanostatic charge/discharge tests were performed on a LAND cycler (WuhanKingnuo Electronic Co., China). Cyclic voltammetry (CV) was performed at different scan rates on a CHI600D electrochemical workstation (Chenhua Instrument, China).

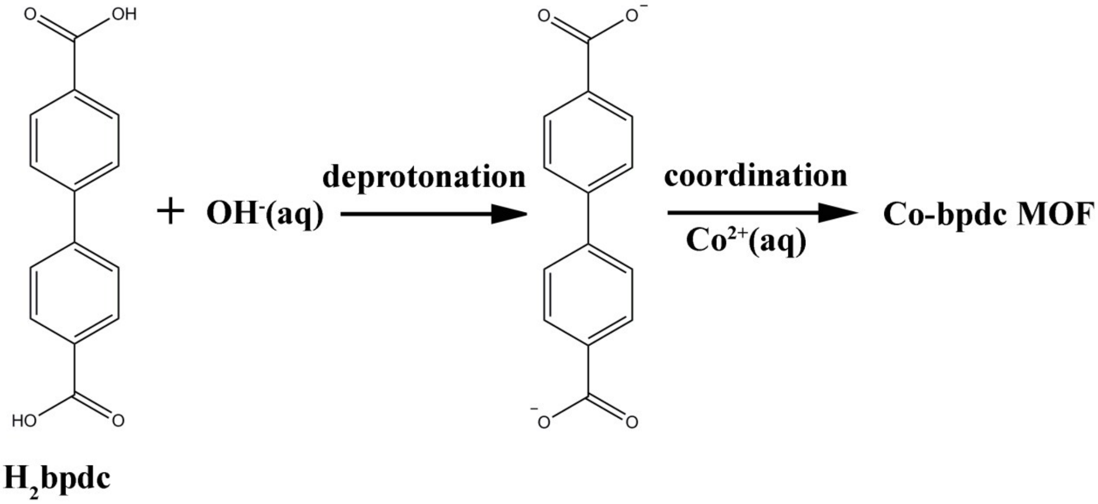

Fig.S1 Synthesis route of Co-bpdc MOF

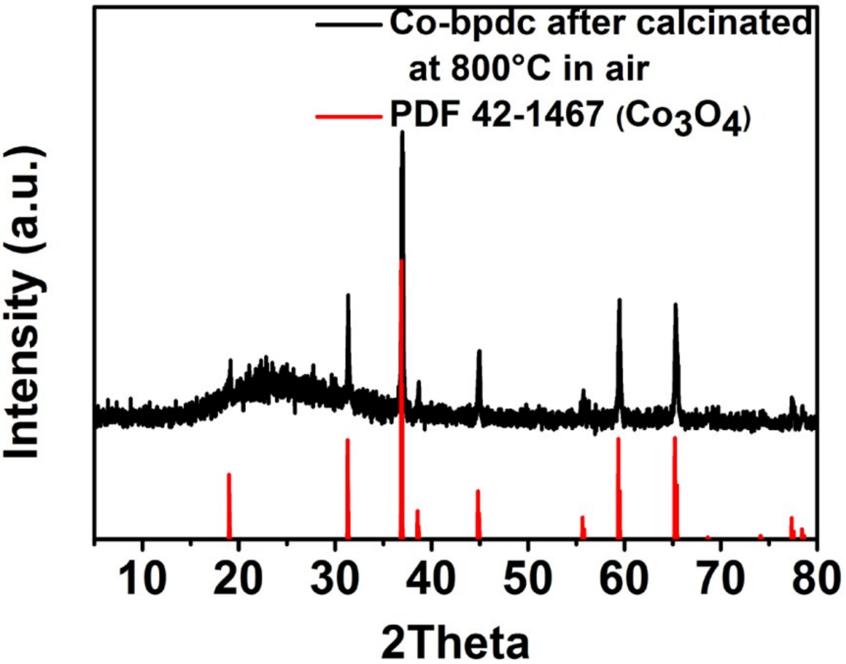

Fig.S2 XRD pattern of Co-bpdc MOF calcinated at 800°C in air.

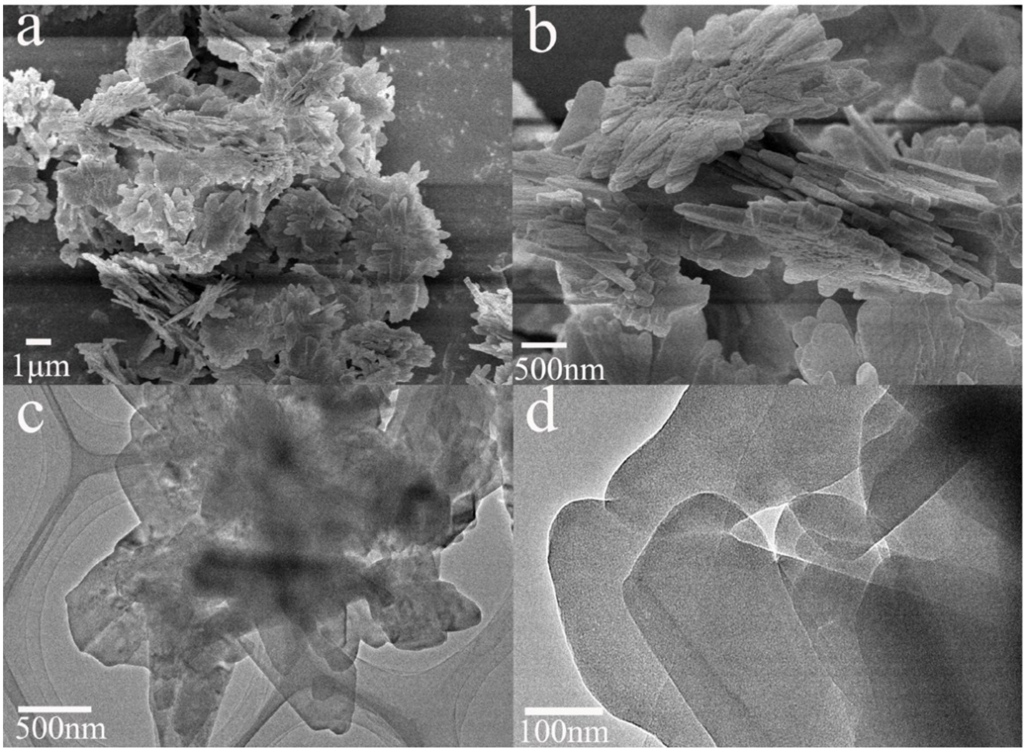

Fig.S3 FESEM and TEM images of the as-prepared Co-bpdc MOF

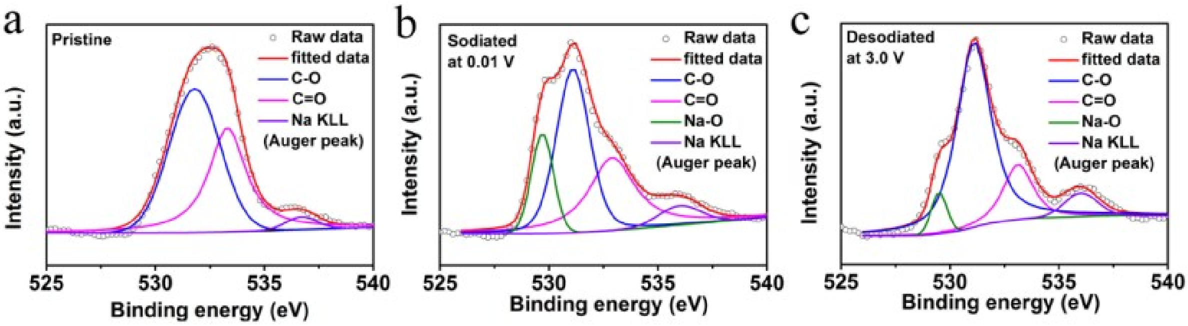

Fig.S4 *Ex-situ* O1s XPS spectra of Co-bpdc electrode during the 1st cycle

At the pristine state, two strong peaks (531.8 eV and 533.3 eV) are attributed to C-O and C=O (in carboxyl) bonds clearly exist.[1, 2] In addition, the Auger peak of sodium (Na KLL) could also be detectable indicating the existence of Na element from electrolytes because the pristine electrode is disassembled and analyzed after assembled and aged together with other cells to make sure the same conditions except for sodiation and desodiation.

At the sodiated state, the relative amount of C=O shows obvious decrease and a new peak located at 529.7 eV and attributed to Na-O bond clearly appears indicating the sodiation of C=O.[3] In the subsequence desodiation process, the relative amount of Na-O bond decreases and that of C=O bond increases indicating the desodiation of Na-O-C to rebuild C=O bond. It is important to note that C=O and Na-O do not disappear in the sodiated and desodiated state, respectively, perhaps due to the existence of PC solvent, CMC binder and the formation of SEI film (such as RCOONa species).

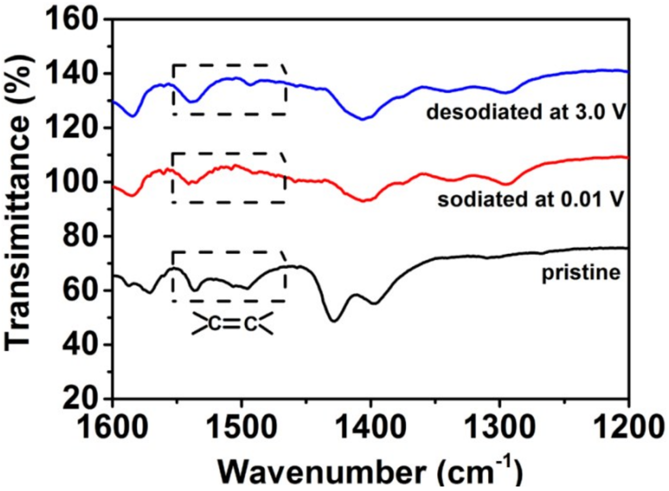

Fig.S5 *Ex-situ* FT-IR analysis of Co-bpdc electrode during the 1st cycle

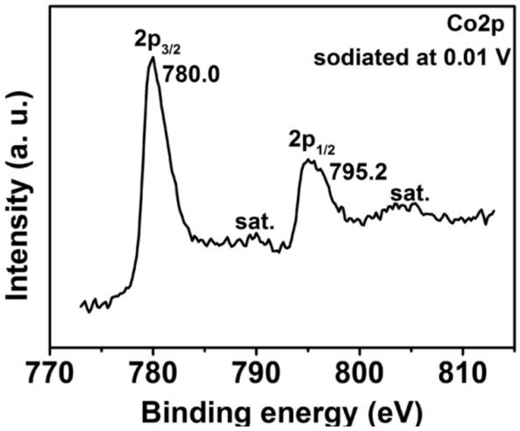

Fig.S6 The Co2p XPS spectra at sodiated state. The Co2p spectra prove the existence of Co(II).[4, 5] This result indicates the Co(II) could not be reduced during the sodiation process and be accord with the sodiation case of other Co-based MOF.[6, 7]

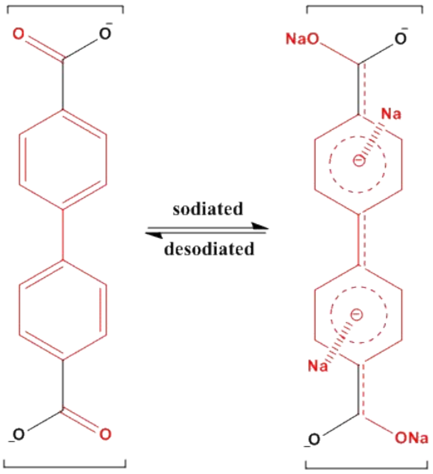

Fig.S7 Proposed redox reaction of Co-bpdc MOF. The theoretical specific capacity is 303.7 mA h g^{-1} (4 Na$^+$, $C_t^S = nF/3.6M_W$).

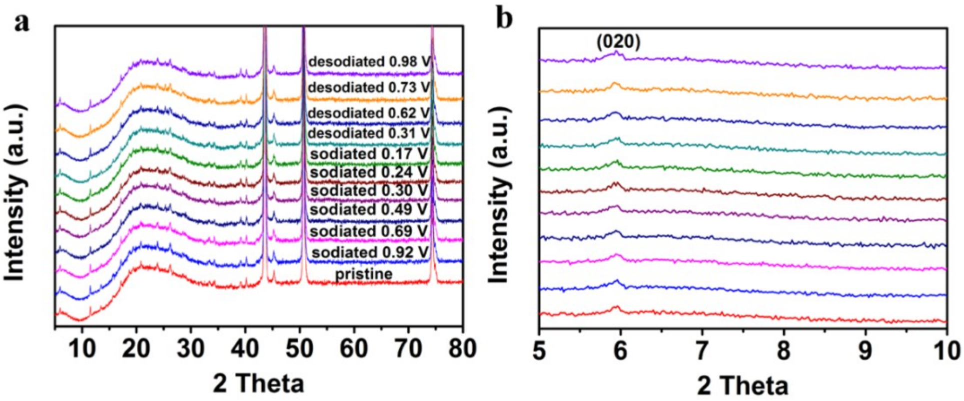

Fig.S8 Selected *ex-situ* XRD patterns during the 1st cycle. As observed, the characteristic of pristine Co-bpdc electrodes remain at different sodiated and desodiated states during the 1st cycle which implies the sodiated and desodiated process of Co-bpdc is not a conversion reaction mechanism. In addition, the location of (020) does not show obvious shift perhaps due to its large lattice space (d_{020}=1.579 nm, much larger than the radius of Na^+).[8] So Co-bpdc does not suffer from too much volume expansion during the sodiation and desodiation process and its large cell volume also facilitates the insertion and extraction of Na^+.

Table S1 Comparison of several crystal parameters between Co-bdc and Co-bpdc

Material	CCDC number	Crystal system	Space group (No.)	Cell volume (Å^3)	Lattice plane perpendicular to ligand	d-spacing (nm)
Co-bdc	163139	monoclinic	C12/c1 (15)	862.5	(200)	0.9034
Co-bpdc	140986	monoclinic	C12/c1 (15)	1359.6	(020)	1.579

By comparing the normal linear ligand (bdc) built MOF (Co-bdc) and our longer linear ligand (bpdc) built MOF (Co-bpdc), they own the same crystal system and space group. However, the bpdc ligand builds larger cell volume and d-spacing. In consideration of the poor electrochemical performances of Co-bdc shown in **Fig.S12**, there are reasons to believe the expanded cell volume and d-spacing of Co-bpdc facilitate the insertion and extraction of Na^+.

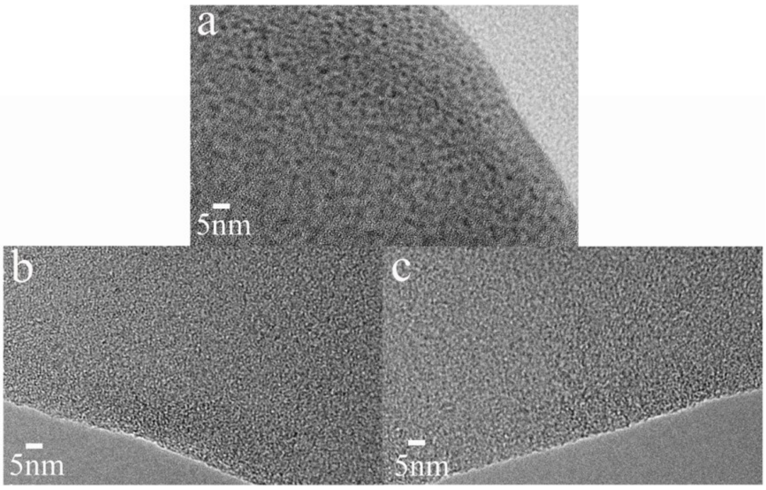

Fig.S9 *Ex-situ* TEM images of Co-bpdc electrode during the 1st cycle. (a) pristine, (b) sodiated at 0.01 V and (c) desodiated at 3.0 V. Observed from the images, no obvious lattice expansion could be found. This indicates the (de)sodiation process do not cause severe structural damage to Co-bpdc and agree well with the *Ex-situ* XRD results.

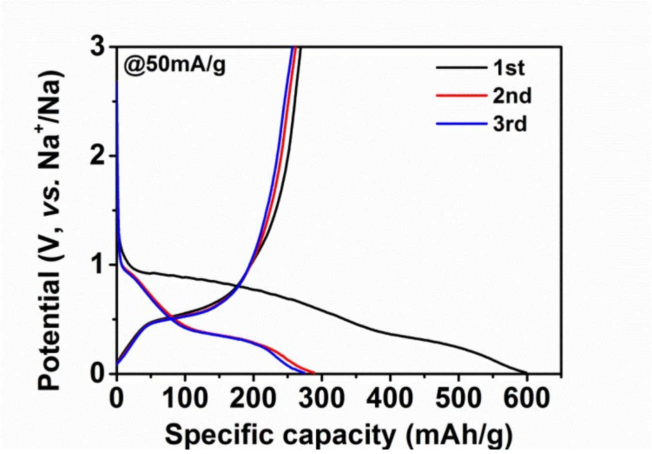

Fig.S10 Voltage profiles of Co-bpdc electrode.

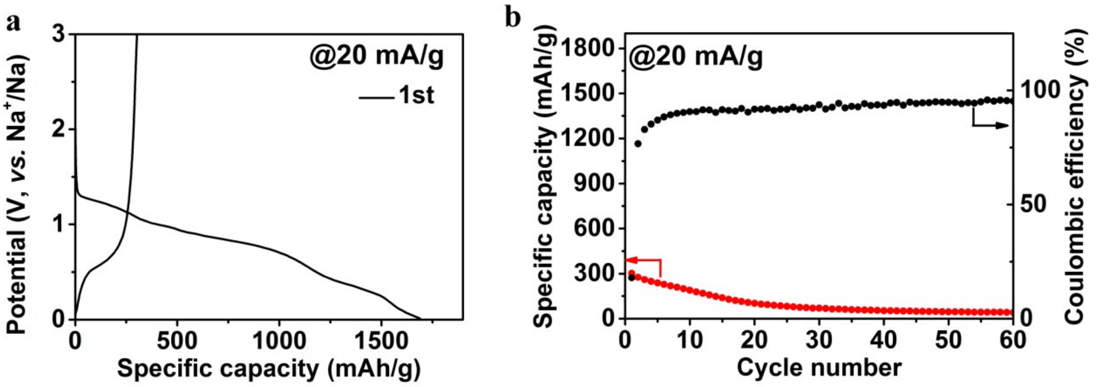

Fig.S11 Electrochemical performances of Co-bpdc electrodes (PVDF as binder and NMP as dispersant).The binder plays important role in the battery systems. As shown in Fig. S2, the Co-bpdc electrodes prepared by PVDF binder displays lower initial Coulombic efficiency and poor cycle performance. Such performances could be related to the poor compatibility between Co-bpdc, PVDF binder and NMP dispersant and agree well with previous reported literature.[9]

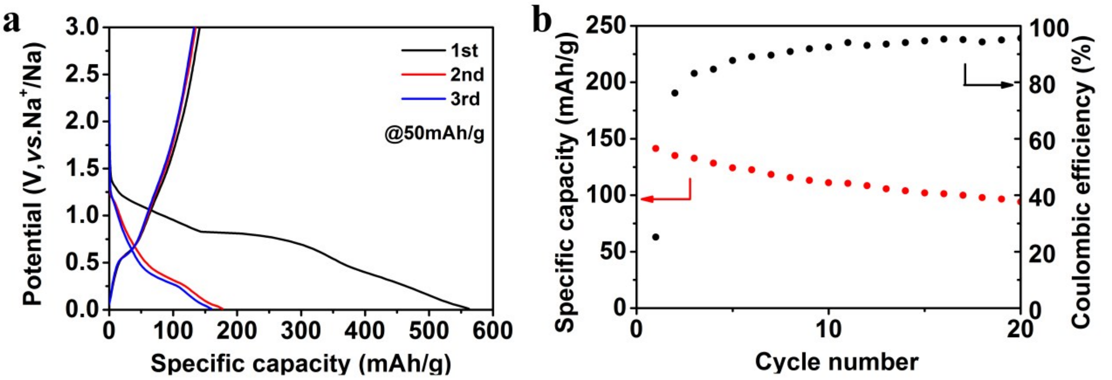

Fig.S12 The sodium storage performances of Co-bdc MOF. The Co-bdc MOF was synthesized as same as Co-bpdc MOF except the ligand. The work electrode preparing and cell testing condition of Co-bdc are also consistent with Co-bpdc. As displayed, the Co-bdc electrodes show poor sodium storage performances perhaps due to the insufficient molecular length of bdc ligand and crowded crystal structure of Co-bdc MOF. This will prove it from another side that the longer linear ligand bpdc and the large cell volume of Co-bpdc facilitate the insertion and extraction of Na^+

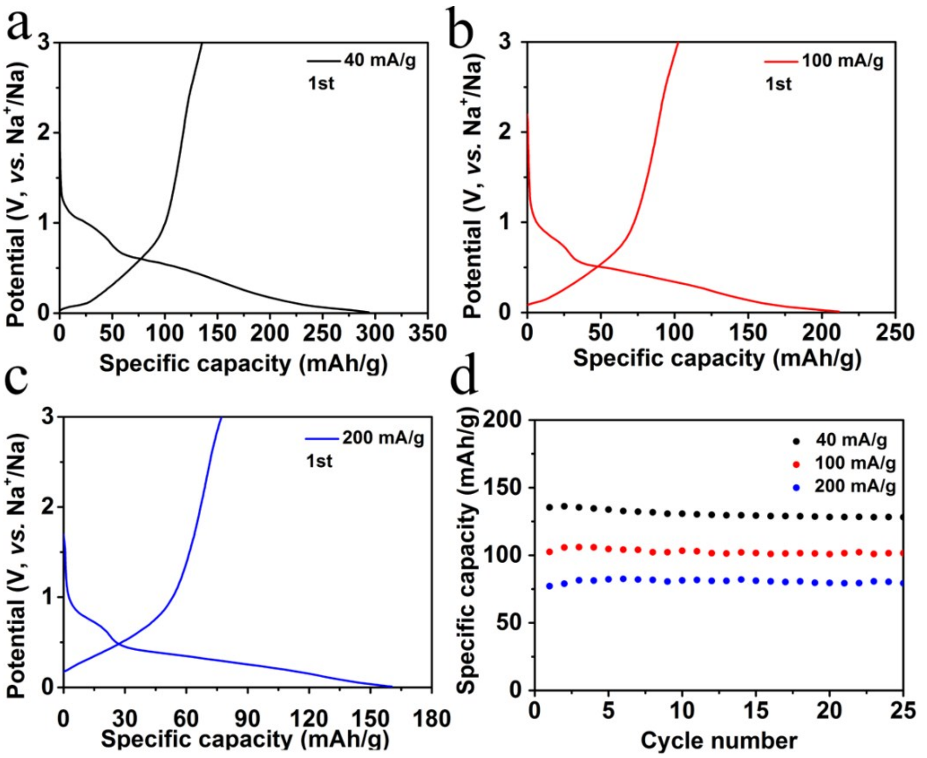

Fig.S13 Voltage profiles and cycle performances (desodiation capacity) of Super P carbon at different current densities. We measured the sodium storage performances of Super P carbon at 40, 100 and 200 mA g^{-1} (corresponding to 20, 50 and 100 mA g^{-1} based on active materials in consideration of their mass ratio of 2:1 in preparation of work electrodes) and the initial capacity contribution of Super P is 68, 51 and 37 mA h g^{-1}, respectively.

Table S2 Performances comparison between Co-bpdc MOF and some reported organic anode materials for SIBs

Materials	Current density (mA/g)	Cycle number	Specific capacity (mA h /g)	Capacity retention (%)	Voltage plateau (V, *vs.* Na^+/Na)	Conductive agent (%)	Test temperature (℃)	Ref
$Na_2C_8H_4O_4$	25.5	50	225	79.8	0.29	26	Not mentioned	10
Na_2TP	30	90	295	90	0.4	37.5	30	11
NaPTCDA	25	100	100	Not mentioned	0.6	20	Not mentioned	12
Ca_2BTEC	20	300	140	Not mentioned	No obvious plateau	30	Not mentioned	13
Na_2BPDC	20.3	150	200	Not mentioned	0.5	28.6	30	14
SSDC	1000	400	112	70	0.39	40	RT	15
NaHBDC	10	50	244	Not mentioned	0.34	30-35	Not mentioned	16
Ag_2TP	141	100	133	79	0.2	30	RT	17
Na_2TP Nanosheets	250	100	105	81	0.24	40	RT	18
Na_2PDC	25.4	100	225	83	0.41, 0.57	35	RT	19
Co-bpdc	**20** **100**	**50** **1000**	**269** **209**	**82** **79**	**0.29**	**30**	**RT**	**This work**

Notes:

1. $C_8H_4O_4^{2-}$, TP and BDC--terephthalic acid; PTCDA--3, 4, 9, 10-perylenetetracarboxylic acid; BTEC--1, 2, 4, 5-benzenetetracarboxylic acid; BPDC--4, 4'-biphenyldicarboxylic acid; SSDC--sodium 4, 4'-stilbenedicarboxylate; Na_2PDC--disodium pyridine-2,5-dicarboxylate.

2. The provided performances of $Na_2C_8H_4O_4$ are performances of the Al_2O_3 coated ALD-20 sample (ALD means atomic layer deposition) reported in Ref 3.

3. RT--room temperature;

References:

1. J.-H. Kang, W.-J. Kwak, D. Aurbach and Y.-K. Sun, *J. Mater. Chem. A*, 2017, **5**, 20678-20686.
2. S.-Y. Lu, M. Jin, Y. Zhang, Y.-B. Niu, J.-C. Gao and C. M. Li, *Adv. Energy Mater.*, 2018, **8**, 1702545.
3. H. W. Nesbitt, G. M. Bancroft, G. S. Henderson, R. Ho, K. N. Dalby, Y. Huang and Z. Yan, *J. Non-Cryst. Solids*, 2011, **357**, 170-180.
4. X. Wei, N. Li and X. Zhang, *Electrochimi. Acta*, 2018, **264**, 36-45.
5. C. Li, X. Hu, X. Lou, Q. Chen and B. Hu, *Chem. Commun.*, 2016, **52**, 2035-2038.
6. C. Dong and L. Xu, *ACS Appl. Mater. Interfaces*, 2017, **9**, 7160-7168.
7. C. Li, X. Hu, X. Lou, L. Zhang, Y. Wang, J.-P. Amoureux, M. Shen, Q. Chen and B. Hu, *J. Mater. Chem. A*, 2016, **4**, 16245-16251.
8. Z. Peng, Q. Wei, S. Tan, P. He, W. Luo, Q. An and L. Mai, *Chem. Commun.*, 2018, **54**, 4041-4044.
9. C. Wang, Y. Fang, Y. Xu, L. Liang, M. Zhou, H. Zhao and Y. Lei, *Adv. Funct. Mater.*, 2016, **26**, 1777-1786.
10. L. Zhao, J. Zhao, Y.-S. Hu, H. Li, Z. Zhou, M. Armand and L. Chen, *Adv. Energy Mater.*, 2012, **2**, 962-965.
11. Y. Park, D.-S. Shin, S. H. Woo, N. S. Choi, K. H. Shin, S. M. Oh, K. T. Lee and S. Y. Hong, *Adv. Mater.*, 2012, **24**, 3562-3567.
12. R. R. Zhao, Y. L. Cao, X. P. Ai and H. X. Yang, *J. Electroanal. Chem.*, 2013, **688**, 93-97.
13. Z. Zhang, H. Yoshikawa and K. Awaga, *Chem. Mater.*, 2016, **28**, 1298-1303.
14. A. Choi, Y. K. Kim, T. K. Kim, M.-S. Kwon, K. T. Lee and H. R. Moon, *J. Mater. Chem. A*, 2014, **2**, 14986-14993.
15. C. Wang, Y. Xu, Y. Fang, M. Zhou, L. Liang, S. Singh, H. Zhao, A. Schober and Y. Lei, *J. Am. Chem. Soc.*, 2015, **137**, 3124-3130.
16. A. Abouimrane, W. Weng, H. Eltayeb, Y. Cui, J. Niklas, O. Poluektov and K. Amine, *Energy Environ. Sci.*, 2012, **5**, 9632.
17. J. Xue, C. Fan, Q. Deng, M. Zhao, L. Wang, A. Zhou and J. Li, *Electrochimi. Acta*, 2016, **219**, 418-424.
18. F. Wan, X.-L. Wu, J.-Z. Guo, J.-Y. Li, J.-P. Zhang, L. Niu and R.-S. Wang, *Nano Energy*, 2015, **13**, 450-457.
19. H. Padhy, Y. Chen, J. Lüder, S. R. Gajella, S. Manzhos and P. Balaya, *Adv. Energy Mater.*, 2018, **8**.